Available online at www.sciencedirect.com
SCIENCE DIRECT
Journal of Power Sources 143 (2005) 256–264
JOURNAL OF POWER SOURCES
www.elsevier.com/locate/jpowsour

The effect of carbon species on the properties of Fe/C composite for metal–air battery anode

Bui Thi Hang[a], Minato Eashira[b], Izumi Watanabe[b], Shigeto Okada[b], Jun-Ichi Yamaki[b,*], Seong-Ho Yoon[b], Isao Mochida[b]

[a] *Interdisciplinary Graduate School of Engineering Sciences, Kyushu University, 6-1 Kasuga-koen, Fukuoka 816-8580, Japan*
[b] *Institute for Materials Chemistry and Engineering, Kyushu University, 6-1 Kasuga-koen, Fukuoka 816-8580, Japan*

Received 18 August 2004; received in revised form 5 November 2004; accepted 16 November 2004

Abstract

For the purpose of finding an adequate carbon additive for a Fe/C composite air battery anode, effects of various carbons on the electrochemical properties of Fe/C composite electrodes were investigated using cyclic voltammetry (CV) and scanning electron microscopy (SEM), together with X-ray energy-dispersive spectroscopy (EDS). Acetylene black, tubular carbon nanofiber (CNF) and platelet CNF exhibited good results, including improved conductivity and higher redox currents of the Fe/C electrode. EDS revealed that on the Fe/nano-carbon surface, especially on the Fe/tubular CNF surface, iron was more dispersed than on Fe/graphite after cycling. Such a high dispersion of iron on nano-carbon surfaces may improve the electrochemical behavior of the Fe redox species.

Keywords: Nano-carbon; Iron/carbon nanocomposite; Air battery anode

1. Introduction

Metal/air batteries have attracted the attention of many researchers because of their high energy density [1–10]. If a metal–air secondary battery system were to become widely utilized, such a battery would likely possess a larger capacity to maintain a high power density than that of a lithium ion battery or a nickel metal hydride battery. A battery's anode is a key factor in deciding its performance, especially its specific capacity and cycle life. For an air battery anode, three kinds of metals are considered to be promising: iron, zinc and aluminum. However, all of these metal anodes have some disadvantages. For example, a zinc anode can experience an inhomogeneous distribution of deposition when charging, which causes the "shape change" phenomenon, with a loss of cycle stability. On the other hand, even though the oxidized species are insoluble in alkali solution, iron anodes suffer from the passivation by iron hydroxide produced by the discharge process. Therefore, increasing interest has been devoted to the development of the anode [11–27]. The reaction mechanism of the iron electrode and the nature of the products formed during the anodic discharge process in alkaline solution have been investigated by several researchers [11–22]. The anodic oxidation of iron proceeds in two main steps, the first of which is [11,13–15,17,20,21]:

$$Fe + 2OH^- \rightarrow Fe(OH)_2 + 2e^- \quad (1)$$

Most authors agree that the formation of $Fe(OH)_2$ is accompanied by the formation of a soluble intermediate product, $HFeO_2^-$ [13,15,17].

The second step involves

$$Fe(OH)_2 + OH^- \rightarrow FeOOH + H_2O + e^- \quad (2)$$

and/or

$$3Fe(OH)_2 + 2OH^- \rightarrow Fe_3O_4 + 4H_2O + 2e^- \quad (3)$$

* Corresponding author. Tel.: +81 92 583 7790; fax: +81 92 583 7790.
E-mail address: yamaki@cm.kyushu-u.ac.jp (J.-I. Yamaki).

0378-7753/$ – see front matter © 2004 Elsevier B.V. All rights reserved.
doi:10.1016/j.jpowsour.2004.11.044

A composite anode of active metals with a nano-sized electronic conductor is expected to improve such problems of metal anodes. For an iron anode, the coexistence of a conductor maintains electrode conductivity even when the anode is in a fully discharged (oxidized) state. In our group, nano-carbon materials have been investigated recently and are assumed to play an important role in electrical energy generation and storage. Carbon is chemically stable and would not participate in a redox reaction, so it is likely that nano-carbons will be used in a composite anode system of metal/air batteries. The effective preparation of a metal/nano-carbon composite should be considered, but first the influence of nano-carbons on the redox behavior of the metal should be confirmed. In the present study, the authors prepared composites of iron and several types of nano-carbon or graphite by mechanical mixing. Through the precise observation of the redox behavior of those composite anodes, we found an interesting additional effect that occurred on an iron/nano-carbon composite. Here the extraordinary additive effect of nano-carbon is also reported.

Table 1
Main characteristics of the carbon materials and iron powder

	Grain size (nm)	BET surface area ($m^2\,g^{-1}$)	True density ($g\,cm^{-3}$)
VGCF	100–300	13	2.21
AB	40–100	68	2.0
Natural graphite	18000	8	2.24
Tube CNF	20–100	92	2.09
Platelet CNF	40–200	91	2.10
Iron	<45000	–	–

2. Experimental

Carbon materials used in this study were as follows: vapor-grown carbon fiber (VGCF; Showa Denko Co.) with an average diameter of ca. 200 nm, acetylene black (AB, Denki Kagaku Co.) with an average diameter of ca. 100 nm, and natural graphite (Chuetsu Graphite Co.) with an average diameter of ca. 18 μm. In addition, we used two kinds of carbon nanofibers (CNFs), of the nanotube type, with an average

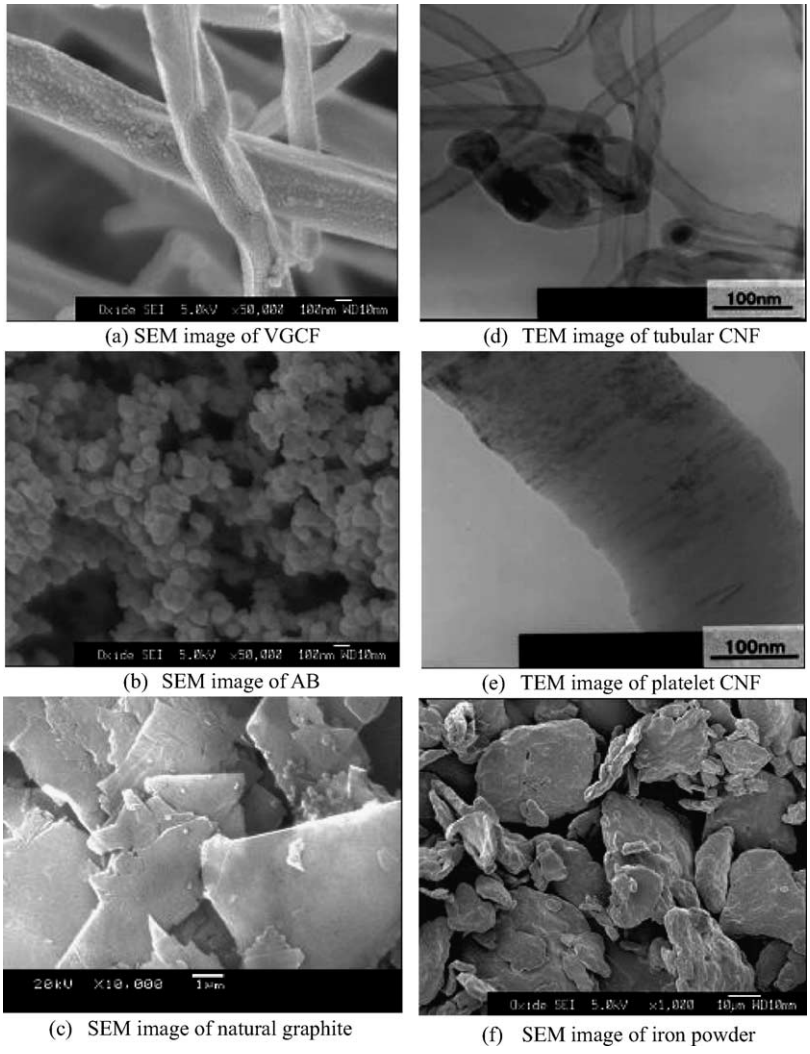

(a) SEM image of VGCF
(d) TEM image of tubular CNF
(b) SEM image of AB
(e) TEM image of platelet CNF
(c) SEM image of natural graphite
(f) SEM image of iron powder

Fig. 1. Morphology of carbon materials and iron powder.

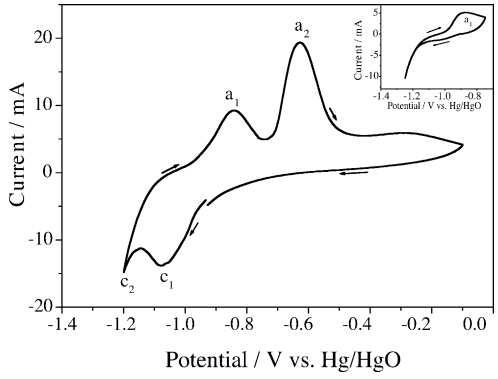

Fig. 2. Voltammogram of iron powder electrode.

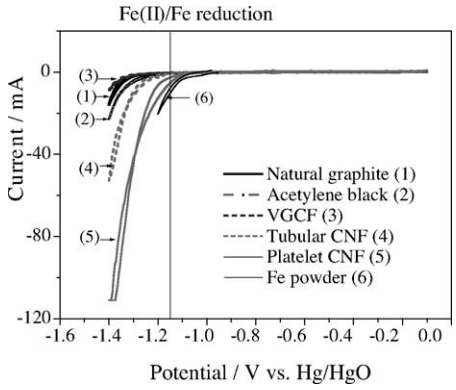

Fig. 3. Cyclic voltammetry of carbon electrodes.

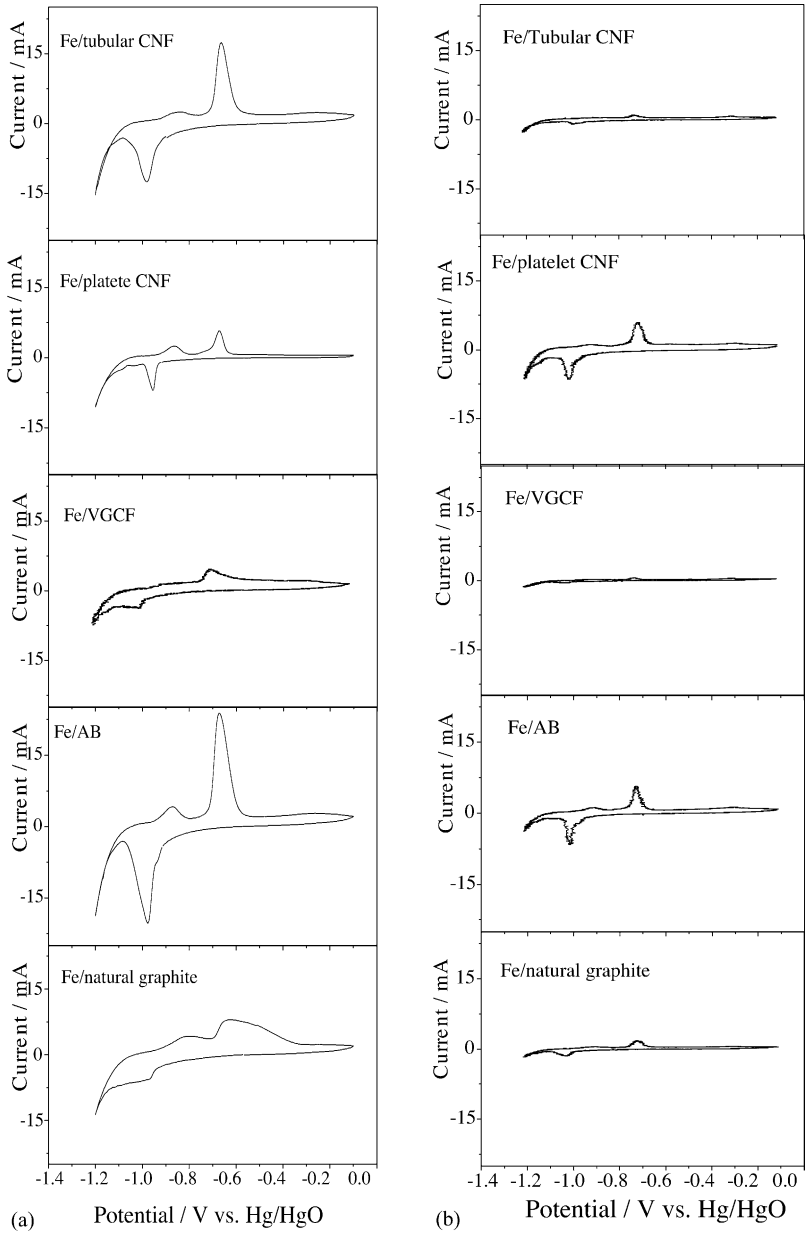

Fig. 4. Voltammograms of Fe/C composite electrodes with Fe:C:PTFE = 45:45:10 wt.% (a) and Fe:C:PTFE = 10:80:10 wt.% (b).

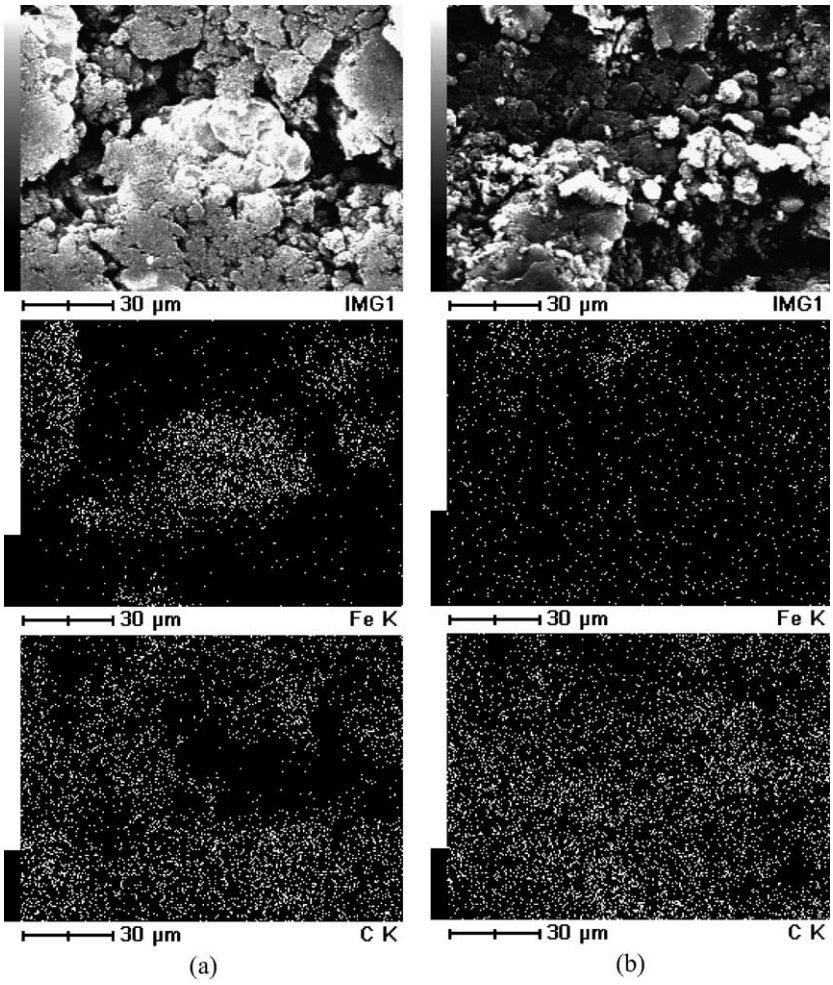

Fig. 5. SEM image and distribution of iron and carbon of Fe/tubular CNF electrode before (a) and after (b) the 15th redox cycle.

diameter of ca. 50 nm, and a platelet type, with an average diameter of ca. 150 nm. In tubular CNF, hexagonal planes compose hollow tubes, while in platelet CNF, a smaller hexagonal plane is stacked perpendicular to a fiber axis. The CNFs were prepared from mixed gases with carbon monoxide over non-supported iron or iron–nickel (Fe–Ni) catalysts, in the temperature range of 560–675 °C using a conventional horizontal tube furnace. The apparatus used for preparation consisted of a quartz flow reactor of 45 mm inner diameter. The total gas flow rate was controlled to be 200 sccm (ml cm^{-3} at 298 K). The gas flow rate in the reactor was precisely monitored and regulated by COFLOC mass flow controllers (COFLOC INC. Tokyo, Japan). The ground passivated catalyst (30 mg) was placed in a quartz boat at the center of the reactor tube in the furnace that had a length of the effective zone of 100 mm. After catalyst reduction in 20 vol.% hydrogen and 80 vol.% of helium (H_2/He = 20/80% v v^{-1}, total 200 sccm) mixtures for 2 h at the desired reaction temperature, helium was flush through the reactor for 0.5 h. The mixed gas of carbon monoxide and hydrogen (CO/H_2) was then allowed to flow over the catalyst for a period of 1 h. The total amount of carbon deposited during the time-on-stream was determined gravimetrically after the reactor was cooled to ambient temperature.

The types of carbons used, excluding graphite, have small average diameters, in the nanometer range, and are hereafter referred to as “nano-carbons”.

Iron powder (Wako Pure Chemical Co.) was used for an iron source. The main characteristics of the carbon materials and iron powder employed are listed in Table 1 and their morphology is shown in Fig. 1.

In order to determine the electrochemical behaviors of each type of carbon or iron, an electrode sheet was prepared by mixing 90 wt.% carbon or iron and 10 wt.% polytetrafluoroethylene (PTFE; Daikin Co.) and rolling. Fe/C composite electrodes, which had two components, were prepared by the same procedure with the mixing ratio of 45 wt.% carbon, 45 wt.% iron powder and 10 wt.% PTFE, or 80 wt.% carbon, 10 wt.% iron powder and 10 wt.% PTFE. The electrode was made into a pellet of 1 cm diameter. The average thickness of electrode was about 0.1 cm. The electrode resistance was determined by use of a digital multimeter (Model 7552, Yokogawa Co.). Cyclic voltammetry was carried out with a three-electrode glass cell assembly that had

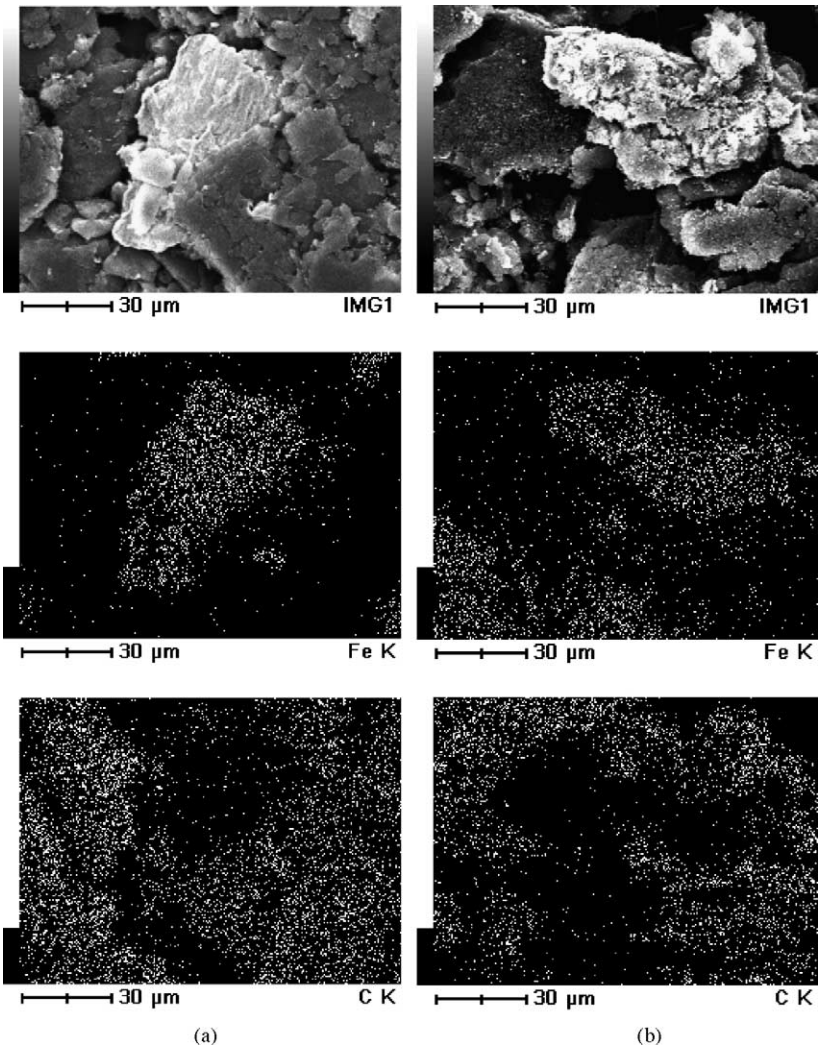

Fig. 6. SEM image and distribution of iron and carbon of Fe/natural graphite electrode before (a) and after (b) the 15th redox cycle.

the carbon or Fe or Fe/carbon composite electrode as the working electrode, silver oxide as the counter electrode and Hg/HgO as the reference electrode. The electrolyte we used was 8 mol dm^{-3} aqueous KOH. Cyclic voltammetry measurements were taken at a scan rate of 0.5 mV s^{-1} and in the range of −1.4 to −0.1 V for carbon electrodes and −1.2 to −0.1 V for Fe or Fe/carbon composite electrodes. After the 15th redox cycle, the Fe/carbon composite electrodes were removed, washed with ion-exchanged water, dried and observed by scanning electron microscopy (SEM) and X-ray energy-dispersive spectroscopy (EDS).

3. Results and discussion

The voltammogram of the iron powder electrode during the second cycle is shown in Fig. 2. Two oxidation peaks were observed around −0.83 V (a_1) and around −0.63 V (a_2). In contrast, only one reduction peak was observable around −1.08 V (c_1), and a hydrogen evolution peak occurred at around −1.2 V (c_2). With further cycling, the redox currents under peaks (a_2) and (c_1) increase in the initial cycles and then decrease. The CV of the iron powder electrode in the range of −1.3 to −0.75 V is also indicated in the inset of Fig. 2. In this voltammogram, only the oxidation peak (a_1) was observed. This indicates that peaks a_2 and c_1 belong to a redox couple. Concerning the CV for the porous iron electrode in 5.35 M KOH + 0.65 M LiOH solution with a sweep rate of 2 mV s^{-1}, Periasamy et al. [20] claimed that during the oxidation process, the conversion of Fe to Fe(II) and Fe(II) to Fe(III) were observed at −0.835 and −0.635 V, respectively. Two reduction peaks were observed at −0.99 and −1.155 V, corresponding to the conversion of Fe(III) to Fe(II) and Fe(II) to Fe. Caldas et al. [22] demonstrated oxidation of the Fe to $Fe(OH)_2$ at −0.88 V and the $Fe(OH)_2$ to Fe(III) at −0.62 V for the porous iron electrode in 6 M KOH + 0.33 M LiOH solution at a scan rate of 0.5 mV s^{-1}. They also observed only one reduction peak of Fe(III) to $Fe(OH)_2$ around −1.0 V. Thus, the anodic peak (a_2) and the cathodic peak (c_1) correspond to the Fe(II)/Fe(III) redox couple. The anodic peak (a_1)

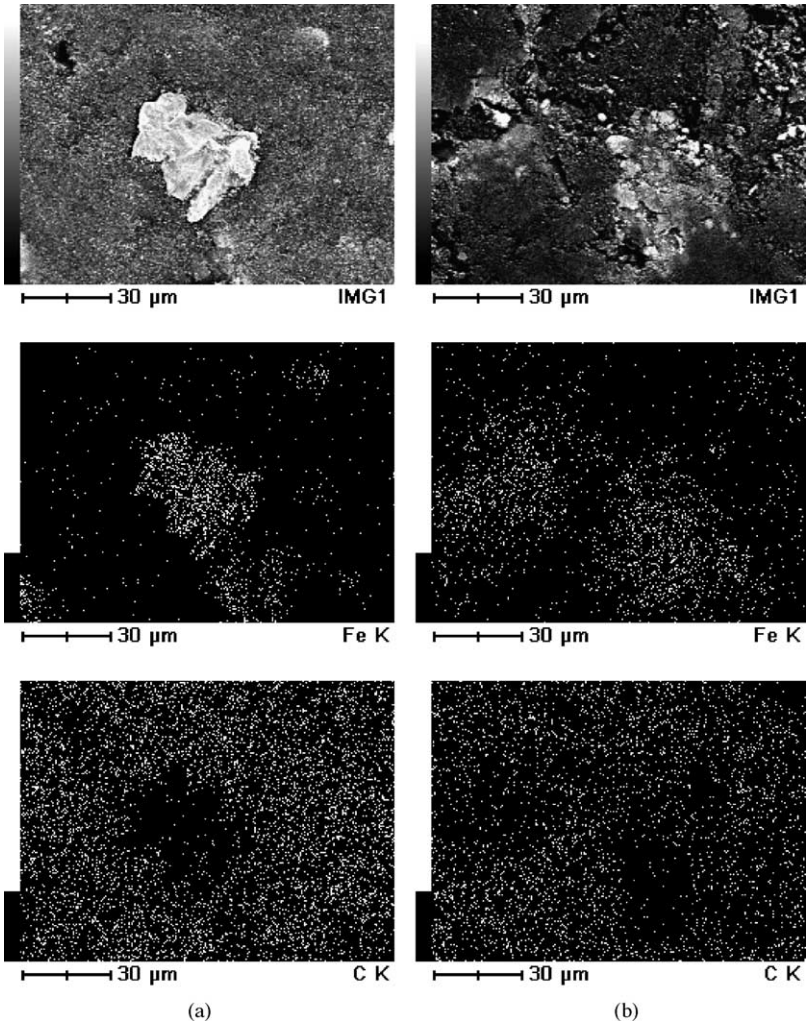

Fig. 7. SEM image and distribution of iron and carbon of Fe/AB electrode before (a) and after (b) the 15th redox cycle.

is attributed to the oxidation of Fe to $Fe(OH)_2$. The cathodic peak corresponding to reduction of $Fe(OH)_2$ to Fe is not visible, probably because it was superimposed on the current for the hydrogen evolution reaction (c_2) [22].

The cyclic voltammograms of the carbon electrodes used in the present study are shown in Fig. 3. It is clear that carbons are not oxidized up to −0.1 V. All carbons show an onset cathodic current, which is attributed to the hydrogen evolution from the electrode surface below −1.1 V. The hydrogen evolution on tubular CNF and platelet CNF occurs at a higher potential than that of natural graphite, VGCF and acetylene black, mainly because the actual surface areas of the nano-carbons are large. In addition, the catalytic effect of the nano-carbon surface, having a different stacking structure of the hexagonal plane and functional groups, may contribute to the hydrogen evolution. In all cases, hydrogen evolution occurs at a sufficiently low potential compared with the Fe redox behavior, and the hydrogen evolution potential on iron is much higher than that on carbon, so that all carbons here are found to be suitable for a Fe/C composite anode.

The resistance measurement results showed that the tubular CNF and VGCF electrode had the smallest resistance values (about 8 Ω), while resistance values of the platelet CNF and AB electrode were about 16 and 13 Ω, respectively. Graphite had the largest resistance value (about 100 Ω). The iron powder electrode had a resistance 1000 times larger than those of all carbon electrodes. When iron was mixed with carbon, the resistance values of the Fe/C electrodes were significantly decreased compared with the iron powder electrode. For example, Fe/tubular CNF electrode, with iron at 45 wt.% had a resistance of about 10 Ω, while a Fe/AB electrode with iron at 45 wt.% had a resistance of about 12 Ω. It is clear that carbon materials improved the conductivity of the Fe/C electrodes.

Fig. 4 shows the cyclic voltammograms of Fe/C composite electrodes with iron at 45 wt.% (a) and 10 wt.% (b). For both contents of iron, the oxidation peaks of Fe/Fe(II) and Fe(II)/Fe(III) were observed around −0.9 and −0.65 V, respectively, while a small reduction peak of Fe(III)/Fe(II) occurred around −1.0 V. Similar to the iron powder electrode, the reduction peaks of iron deposition and hydrogen evolution

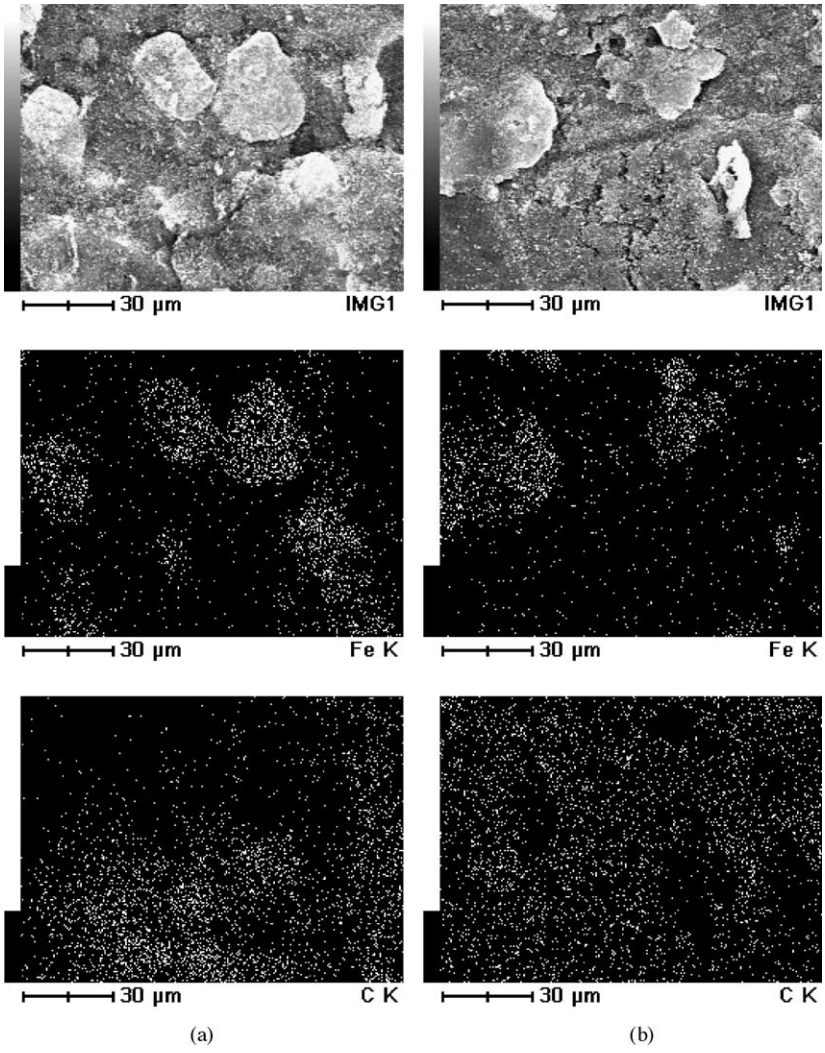

Fig. 8. SEM image and distribution of iron and carbon of Fe/platelet CNF electrode before (a) and after (b) the 15th redox cycle.

were not observed separately with various carbon additives. With further cycling the redox current of the Fe(II)/Fe(III) couple of the Fe/C electrode was increased. In contrast to the iron electrode, the redox current of the Fe(II)/Fe(III) couple decreased with repeated cycling. From these profiles it is clear that the carbon component affects the redox behavior of iron. For example, compared with the iron powder electrode, platelet CNF and acetylene black provided a sharp reduction peak for Fe(III)/Fe(II) around −1.0 V and a corresponding oxidation peak around −0.65 V, with a small oxidation peak for Fe/Fe(II) around −0.9 V. Furthermore, the reduction peak of Fe(III)/Fe(II) was separated sufficiently from the hydrogen evolution peak around −1.2 V compared with the corresponding reduction peak in the iron powder electrode. If the carbon component was tubular CNF, only when the iron ratio was 45 wt.% did such peaks appear clearly. In the case of VGCF and natural graphite composites, the applied peaks were rather small, and the reduction peak for Fe(III)/Fe(II) was not separated sufficiently from the hydrogen evolution peak. When the iron content was 10 wt.%, the peak current decreased markedly, except in the case of the Fe/platelet CNF composite.

This behavior is acceptable from the viewpoint that nanocarbons should have a larger actual surface area than graphite and therefore the $Fe(OH)_2$ layer formed via intermediate species on the nano-carbon surface should be thinner than that on graphite. This $Fe(OH)_2$ layer is easily oxidized to Fe(III) on the nano-carbon surface, while only the thin outer layer of $Fe(OH)_2$ was oxidized to Fe(III) on graphite, and thus a passive layer was formed. Such a thin-layer distribution of Fe(III) on the nano-carbon surface resulted in a small resistance of the electrode pellet. Consequently, we assume that some Fe species may be distributed uniformly, particularly on a nano-carbon surface throughout the electrochemical dissolution/deposition process of Fe, and consequently the active surface area may increase. In order to confirm the mode of distribution of iron on each carbon, EDS measurements, together with SEM observations were carried out.

Figs. 5–9 show the SEM images and distributions of iron and carbon by EDS on the surfaces of the Fe/tubular CNF,

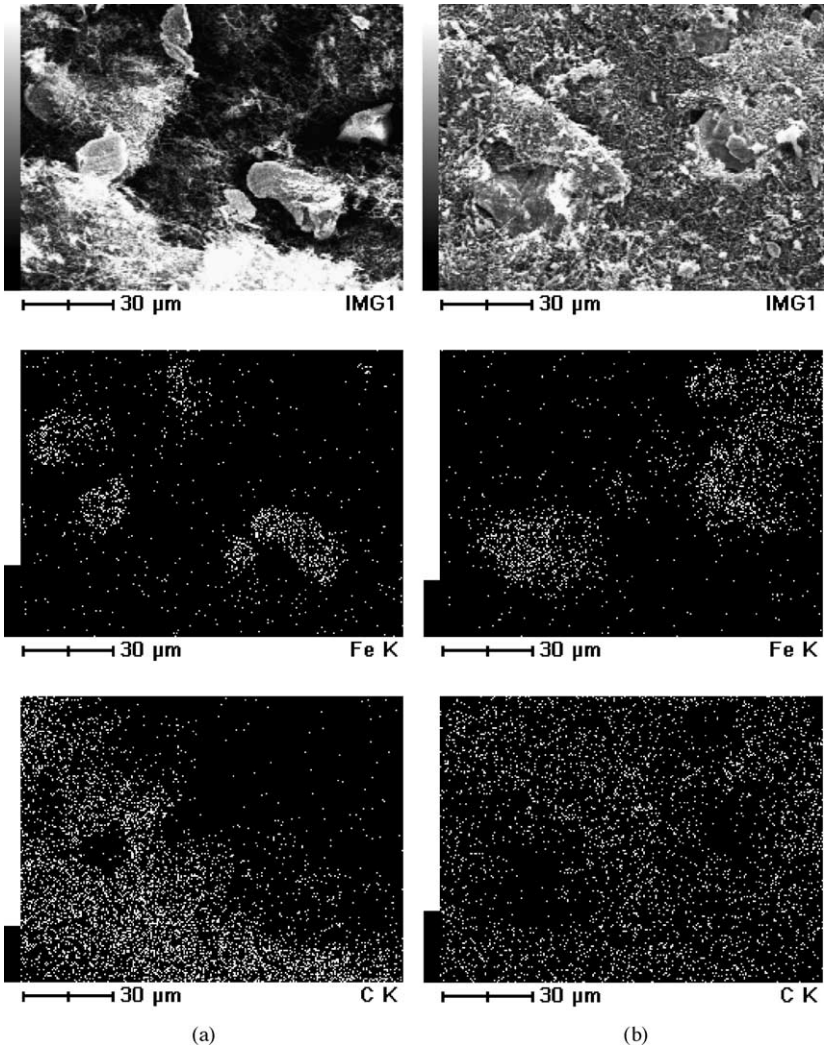

Fig. 9. SEM image and distribution of iron and carbon of Fe/VGCF electrode before (a) and after (b) the 15th redox cycle.

Fe/natural graphite, Fe/AB, Fe/platelet CNF and Fe/VGCF composite electrodes before and after the 15th cycle. Before that cycle, most iron species were only observed as particles that were tens of micrometers in size. After the 15th cycle, when mixed with graphite, the iron was dispersed only a small amount. In contrast, when mixed with nano-carbon materials, especially tubular CNF, the iron dispersed more via charge–discharge cycles. However, among the nano-carbon materials employed, Fe/tubular CNF and Fe/AB showed the greater dispersion of iron compared to other nano-carbons, mainly because their actual surface areas are larger than those of other nano-carbon materials. This dispersion must be due to the deposition/dissolution coupled with the redox cycles of iron. Periasamy et al. [20] claimed that an intermediate Fe redox species, $HFeO_2^-$, is soluble, even in alkali solutions. In this case such an intermediate may play a main role in iron dispersion. It is important to reveal the origin of the difference in iron dispersion on the nano-carbon surface, for example, on a tubular CNF surface and on a graphite surface. One possible explanation is the dependence of the morphology of the carbon surface on the distribution of iron during the charge/discharge. In the case of a Fe/nano-carbon electrode, the distance between iron and carbon species is expected to be shorter than in the case of Fe/graphite, in which case the amount of dispersed iron on a nano-carbon surface would be larger than that on graphite. Moreover, a nano-carbon surface area, on which Fe would be distributed, is also larger than that of graphite. In addition, the dependence for the morphology of the carbon surface on the diffusion of dispersed iron species supports the above explanation. For example, it is expected that the diffusion path of mobile iron between an iron particle and tubular CNF is much shorter than that between an iron particle and graphite. Furthermore, some special effects caused by the surface structure or composition of some nano-carbons can be expected. The mechanism for such high iron dispersion is to be further investigated in a future study.

4. Conclusion

Nano-carbons affect the electrochemical properties of Fe/C composite electrodes. Acetylene black, tubular CNF

and platelet CNF, based on their large actual surface areas, showed improved conductivity, producing higher redox currents for the Fe/C electrodes and provided a Fe(III)/Fe(II) reduction peak sufficiently separated from the hydrogen reduction peak. However, the reduction peaks of iron deposition and hydrogen evolution were not observed separately with various carbon additives.

On the Fe/nano-carbon surface, especially on the Fe/tubular CNF surface, which has a special structure, i.e., a large actual surface area, iron was more dispersed than on Fe/graphite.

Acknowledgement

This work was supported by the CREST program of JST (Japan Science and Technology Agency).

References

[1] L. Ojefors, L. Carlsson, J. Power Sources 2 (1977/1978) 287–296.
[2] K.F. Blurtin, A.F. Sammells, J. Power Sources 4 (1979) 263–279.
[3] A.M. Kannanand, A.K. Shukla, J. Power Sources 35 (1991) 113–121.
[4] S. Muller, F. Holzer, O. Haas, J. Appl. Electrochem. 28 (1998) 895–898.
[5] J. Goldstein, I. Brown, B. Koretz, J. Power Sources 80 (1999) 171–179.
[6] M. Maja, C. Orecchia, M. Strano, P. Tosco, M. Vanni, Electrochim. Acta 46 (2000) 423–432.
[7] Z. Wei, W. Huang, S. Zhang, J. Tan, J. Power Sources 91 (2000) 83–85.
[8] K. Akuto, Y. Sakurai, J. Electrochem. Soc. 148 (2001) A121–A125.
[9] X. Wang, P.J. Sebastian, M.A. Smit, H. Yang, S.A. Gamboa, J. Power Sources 124 (2003) 278–284.
[10] W.H. Zhu, B.A. Poole, D.R. Cahela, B.J. Tatarchuk, J. Appl. Electrochem. 33 (2003) 29–36.
[11] A.J. Salkind, C.J. Venuto, J. Electrochem. Soc. 111 (1964) 493–495.
[12] L. Ojefors, J. Electrochem. Soc. 123 (1976) 824–828.
[13] L. Ojefors, J. Electrochem. Soc. 123 (1976) 1691–1696.
[14] R.S. Schrebler-Guzman, J.R. Viche, A.J. Arvia, Electrochim. Acta 24 (1979) 395–403.
[15] N. Jayalakshimi, V.S. Muralidharan, J. Power Sources 32 (1990) 277–286.
[16] M.D. Koninck, T. Brousse, D. Belanger, Electrochim. Acta 48 (2003) 1425–1433.
[17] J. Cerny, J. Power Sources 25 (1989) 111–122.
[18] D.W. Shoesmith, P. Taylor, M.G. Bailey, B. Ikeda, Electrochim. Acta 23 (1978) 903–916.
[19] T.S. Balasubramanian, A.K. Shukla, J. Power Sources 41 (1993) 99–105.
[20] P. Periasamy, B. Ramesh Babu, S. Venkatakrishma Iyer, J. Power Sources 58 (1996) 35–40.
[21] P. Periasamy, B. Ramesh Babu, S. Venkatakrishma Iyer, J. Power Sources 63 (1996) 79–85.
[22] C.A. Caldas, M.C. Lopes, I.A. Carlos, J. Power Sources 74 (1998) 108–112.
[23] J. Huot, E. Boubour, J. Power Sources 65 (1997) 81–85.
[24] J. Zhu, Y. Zhou, C. Gao, J. Power Sources 72 (1998) 231–235.
[25] J. Zhu, Y. Zhou, J. Power Sources 73 (1998) 266–270.
[26] R. Shivkumar, G.P. Kalaignan, T. Vasudevan, J. Power Sources 55 (1995) 53–62.
[27] R. Shivkumar, G.P. Kalaignan, T. Vasudevan, J. Power Sources 75 (1998) 90–100.